Carbonation rate of compacted recycled aggregates for sub-base layers of pavement

Yunlu Hou, Pierre-Yves Mahieux, Jérôme Lux, Philippe Turcry, Abdelkarim Aït-Mokhtar

Version of Record: https://www.sciencedirect.com/science/article/pii/S0950061821031603
Manuscript_0535bcf2f0eacafaed66bb20f9339302

Carbonation rate of compacted recycled aggregates for sub-base layers of pavement

Yunlu HOU[1, 2, *], Pierre-Yves MAHIEUX[1], Jérôme LUX[1], Philippe TURCRY[1], Abdelkarim AÏT-MOKHTAR[1]

[1] Laboratoire des Sciences de l'Ingénieur pour l'Environnement (LaSIE), UMR CNRS 7356, La Rochelle Université, Avenue Michel Crépeau, 17000 La Rochelle, France.

[2] Agence de l'environnement et de la maîtrise de l'énergie (ADEME), 20 avenue du Grésillé-BP 90406 49004 Angers cedex 01, France.

* Corresponding author: yunlu.hou1@univ-lr.fr

Abstract

Recycled aggregates are mainly composed of demolition concrete aggregates, i.e., reactive materials that can bind CO_2. The aim of the present study was to investigate the carbonation of recycled aggregates after compaction for road layers construction. Experiments were carried out on samples of compacted recycled sand kept in various moisture conditions. Carbonation was investigated by means of pH indicator spraying, thermogravimetric analysis and CO_2 diffusion tests. The results show that the carbonation rate of compacted recycled aggregates is of the order of about ten millimetres per year$^{1/2}$. Recycled aggregates after compaction constitute a significant carbon sink since a maximum of 30kg of CO_2 is bound per m^3. However, from an application point of view, it seems preferable to carbonate the recycled aggregates before they are placed in their final environment to achieve all benefits of carbonation.

Keywords: Recycled aggregates, compacted recycled sand, carbonation, CO_2 uptake, road construction

1 Introduction

Recycled Aggregates (RA) are made from the crushing and screening of inert construction and demolition waste (CDW) in recycling platforms. Generally, RA are mainly made up of demolition concrete aggregates (old cement paste and natural aggregates), natural aggregates (NA), and, to a lesser extent, contain bitumen aggregates, brick, glass, wood, and plastic [1]. Many studies have documented RA as an alternative material that could be reused in road construction [2–4].

Garach et al. [5] showed that the soaked California Bearing Ratio (CBR) of compacted recycled aggregates increased over time. This increase of mechanical strength is usually attributed to hydration reactions or pozzolanic reactions [4–7]. According to Poon et al. [8], the anhydrous cement in the adhered mortar of fine recycled concrete aggregates is the reason for the self-cementing properties of sub-base materials. Vegas et al. [6] reported that the presence of ceramic materials in RA induces pozzolanic reactions which increase the bearing capacity of the compacted RA.

In addition to these potential reactions, the cementitious matrix can also react with atmospheric CO_2. Cement hydrates react with CO_2 dissolved in water to form calcium carbonate ($CaCO_3$) [9–11]. The carbonation is related to the quality of concrete, exposed surface, and exposure time. In the field of durability of reinforced concrete structures, there is abundant literature on concrete carbonation, because this phenomenon is a major cause of rebars corrosion. Carbonation was also studied in the case of RA. Most of the papers published on RA deal with the CO_2 curing used to improve their properties, e.g. [11–16]. Carbonation reduces both porosity and water absorption of RA, what is conducive to their reuse in concrete [14,17]. It should be noted that the RA studied in these works are mainly composed of recycled concrete aggregate.

In the last few years, several studies have worked on CO_2 sequestration through carbonation of crushed concrete [13,14,17]. The rate of CO_2 uptake and the amount of CO_2 bound by the RA are dependent on mainy parameters. CO_2 uptake increases with a decrease of RA size due to a larger exposed surface [11,17,18]. The water content of adhered mortar in RA is a parameter that has a

great influence on carbonation kinetics of RA [19,20]. A relative humidity between 40% and 70% creates a favorable environment for carbonation of RA [17]. Additionally, the CO_2 uptake increases when increasing the ambient CO_2 concentration [21]. Xuan et al. [14] found that, at a CO_2 concentration of 100%, RA bound more CO_2 at a pressure of 5 bar than at a pressure of 0.1 bar. Most of the literature showed that the rate of carbonation increases with temperature. The optimal temperature for carbonation is between 50°C and 80°C, depending on the type of cement [22].

Even if it seems impossible to carbonate all the calcium oxides contained in hydrates of cement [19], Lippiatt et al. [23] pointed out that carbonation of recycled concrete aggregates might be one of the most promising solutions to reduce the carbon footprint of concrete. Several studies proposed orders of magnitude estimation of the CO_2 uptake capacity of RA. Kikuchi and Kuroda [11] found that 1 kg of RA bind approximately 10 g of CO_2 thanks to atmospheric carbonation. Sereng [20] found that 1 kg of recycled concrete aggregates binds up to 50 g of CO_2 at 20°C with a partial pressure of CO_2 of 15%.

The carbonation of RA was mainly studied at the aggregate scale, but, to our knowledge, there has been no work on the carbonation of compacted RA in road construction. Compacted recycled aggregate, hereafter denoted CRA, is a potentially reactive porous medium. This study aims at evaluating the carbonation rate and the CO_2 binding capacity of CRA. These data are indeed of great interest for predicting the time evolution of sub-base layers of pavement and their CO_2 uptake.

2 Materials

2.1 Raw materials

The studied material is a 0/6 mm fine recycled aggregate produced on a recycling platform in La Rochelle (France). The study focused on fine aggregate as the latter has *a priori* the highest potential reactivity. On-site, construction and demolition wastes were crushed and screened then stored before testing in laboratory. The RA were sorted manually according to the European Standard NF EN 933-

11 [24]. The particle fraction higher than 4 mm is made up of 82.9 % demolition concrete aggregates (Rc), 16.3% natural aggregates (Ru), and aggregates of glass and tiles (Rg) in minor proportions (Table 1).

Table 1: Constituent of 4/6 mm RA in accordance with the European Standard NF EN 933-11 [24].

Description of constituents	Mass proportion (%wt.)
Rc (concrete, concrete products, mortar, concrete masonry units)	82.9
Ru (unbound aggregate, natural stone, hydraulically bound aggregate)	16.3
Ra (bituminous materials)	0.0
Rb (clay masonry units, calcium silicate masonry units, aerated non-floating concrete)	0.1
Rg (glass)	0.6
X (other: metals, non-floating wood, plastic, gypsum plaster, etc.)	0.1

2.2 Sample preparation

Three types of CRA cylindrical samples were made for this study, with 5 cm diameter (ϕ) and 1, 2, or 5 cm height (H),. RA were preliminarily dried at 105°C for 48h then placed in the room to cool. The initial water content (w_i) of RA was about 1%. After oven-drying, for each sample, RA was mixed with 10% water content. In accordance with the European Standard NF EN 13286-53 [25], the resultant mix was compacted, then extruded by axial compression (Figure 1). The dried RA mass and the total water content (inter and intra-granular water) were fixed to have an initial compressive strength equal to 1 MPa. This value corresponds to the compressive strength for authorising road traffic during construction [26].

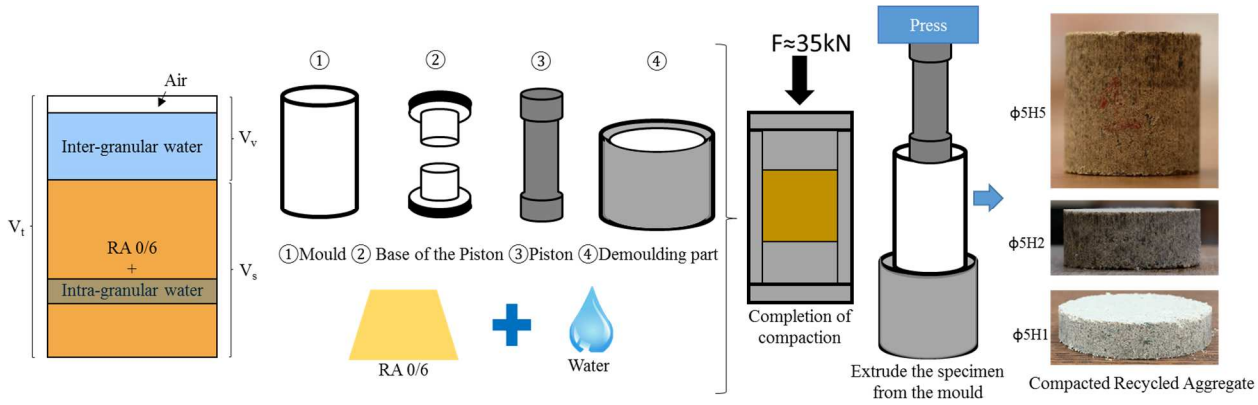

Figure 1: Preparation process of CRA cylindrical samples.

Table 2: Dimensions and composition of the CRA samples.

Sample height (cm)	Designation	Vt (cm^3)	Vs (cm^3)	Vv (cm^3)	RA 0/6 (g)	Water (g)	w_i (%)	w_a (%)	C (%)
5	CRA-H5	98.2	67.4	30.8	170.3	17.0			
2	CRA-H2	39.3	27.0	12.3	68.1	6.1	1	10	0.69
1	CRA-H1	19.6	13.5	6.1	33.7	3.4			

Note: Vt-total volume; Vs-volume of solids; Vv-volume of voids, w_a-content of water added; C-Compactness.

2.3 Curing conditions

More than 240 CRA samples were stored over one year at 20±2°C in four enclosures (Table 3). The three so-called natural carbonation enclosures were placed at three relative humidities (53%, 65%, and 95%). These relative humidities (RH) were chosen to favour, or not, the diffusion of CO_2 in the inter and intra-granular porosity in natural concentration (CO_2 concentration around 0.05%). In the fourth so-called accelerated carbonation enclosure, the RH was fixed at 65±5% which is *a priori* favourable to natural carbonation. The CO_2 concentration was increased from ~0.05% to 3% as soon as the mass of CRA was stabilised (relative mass variation < 0.1%) (Figure 2(b)). A ventilator was placed on the top to homogenise the CO_2 concentration throughout the enclosure.

For all enclosures, the relative humidity was controlled by saturated salt solutions with magnesium nitrate for 53.5% RH, ammonium nitrate for 65% RH, and demineralised water for 95% RH. Table 3 and figure 2 summarise all parameters for curing conditions.

Table 3: Curing conditions of specimens.

Curing conditions	Designation	RH (%)	CO_2 concentration
Natural carbonation (a)	53Nat	53.5±5	≈0.05%
	65Nat	65±5	
	95Nat	95±5	
Accelerated carbonation (b)	65Acc	65±5	≈0.05% then 3%

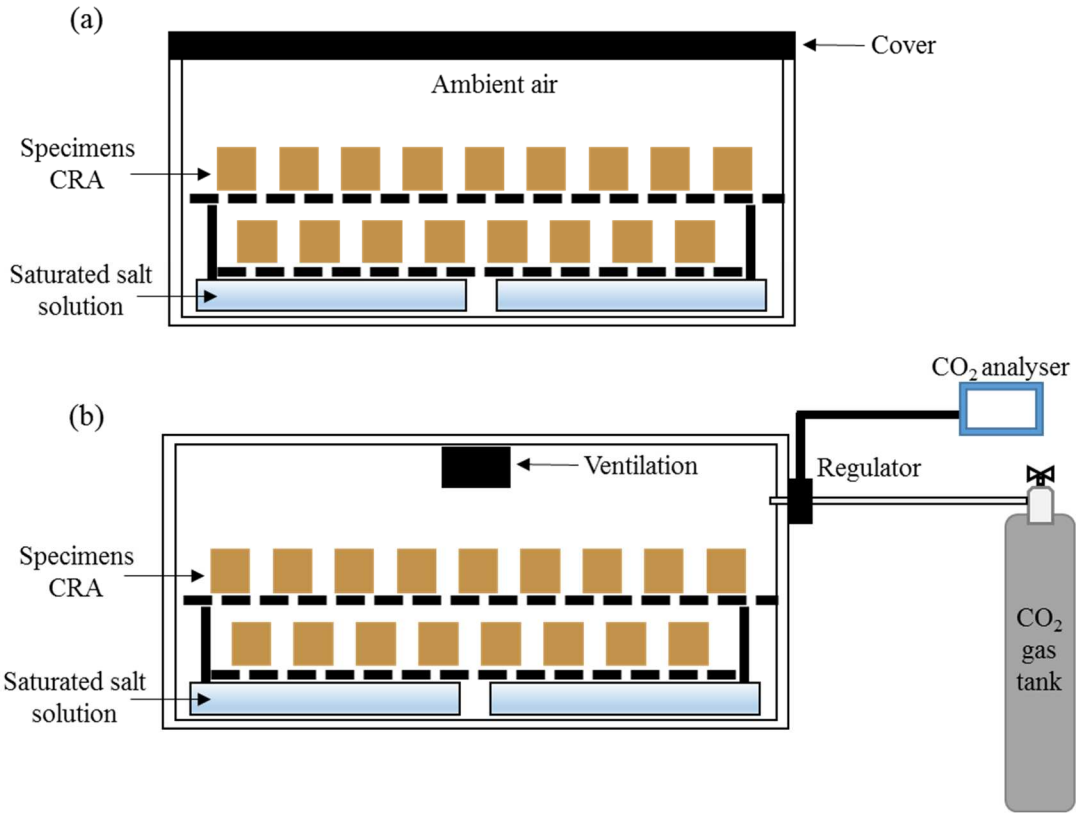

Figure 2: (a) Experimental setup of CO_2≈0.05% at 53.5%, 65% and 95% RH; (b) Experimental setup of CO_2=3% curing at 65% RH.

3 Methods

3.1 Water vapour desorption isotherm

Two test methods were used to determine water vapour desorption isotherms:

- GSA method: A multisample Gravimetric Sorption Analyser (ProUmid GmbH instrument) with automatic weigthing system was used to test samples of CRA-H1 and RA. The mass of the samples was equal to around 190 g. Seven drying steps were performed at 20°C from

90% to 0% RH. The equilibrium criterium between tow steps was a mass variation lower than 0.005% during 180 minutes. The drying steps lasted up to a month.

- SSS method: The CRA-H5 samples in the three enclosures in natural conditions (53 Nat, 65 Nat, and 95 Nat) were weighed periodically for more than two years. Mass loss ε in g/cm^3 was calculated as follows:

$$\varepsilon = \frac{m_i - m_t}{V_t} \text{ (g/cm}^3\text{)} \qquad (1)$$

where V_t is the apparent volume of the sample, m_i is the initial mass, and m_t is the mass at time t. The water content equilibrium was assumed to be reached when the mass variation between two measurement times was less than 0.1% over 7 days, after which the water content was determined with an oven drying at 105°C for 24h.

Some samples of all materials, CRA and RA, were immerged in distilled water for 48 hours under vacuum to determine the water content at saturation and thus to estimate the water content at 100% RH.

An additional test was carried on CRA-H5 drying at 53% RH to determine radial profiles of water content, from the drying surface to the core, at four times (0, 7, 30, and 300 days). At each time, the average water contents were determined on three slices that were gradually nibbled along the radial direction: 0-8 mm, 8-16 mm, and 16-25 mm, as shown in Figure 3.

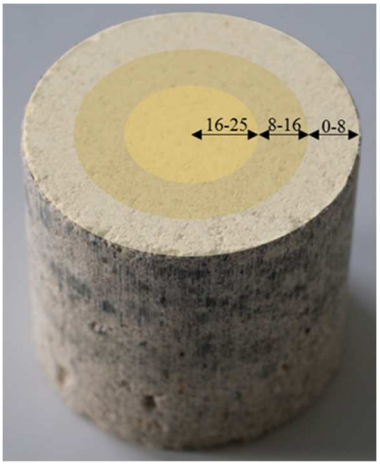

Figure 3: View of a CRA specimen showing the three slices used for determination of water content (0-8 mm; 8-16 mm and 16-25 mm)

3.2 Carbonation depths

The carbonation depths Xc of CRA-H5 samples from all enclosures were determined at different times by spraying of a phenolphthalein alcoholic solution on the cross-sections. The latter were obtained by splitting the cylindrical samples.

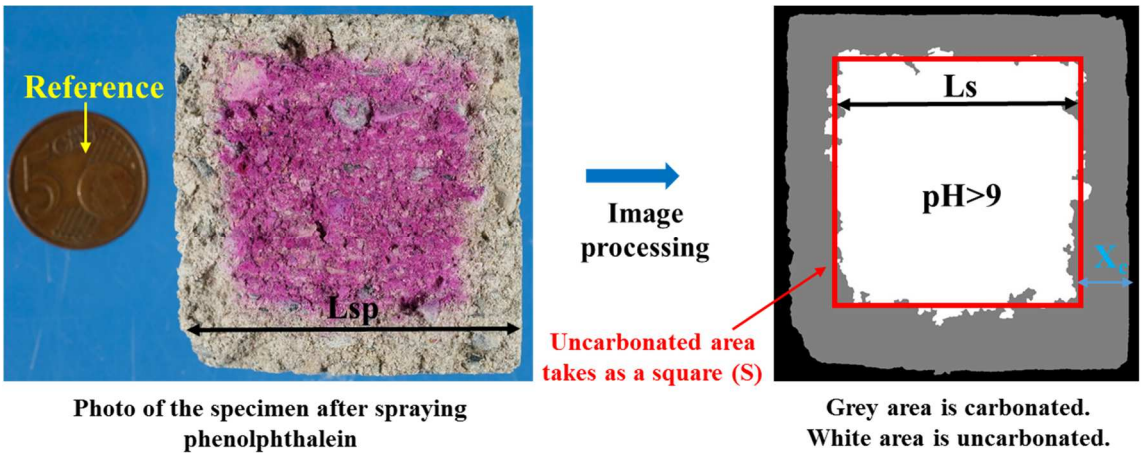

Figure 4: Image analysis of the carbonated area for the determination of the carbonation depth.

The colour indicator solution presents an uncoloured area where the pH is less than 9, which is assumed to be a carbonated area. As shown in Figure 4, pictures were taken with a Fujifilm X-T20 camera to evaluate the average carbonation depth. The images are first binarized using a colour threshold in LAB colour space. After filtering noise, the surface of the non-carbonated area (S) is

measured. Here we use a 5 euro cent coin to calibrate the pixel size. Using this surface, we can calculate an average carbonation depth X_c using the following equation:

$$X_c = \frac{Lsp - Ls}{2} \quad (2)$$

where $L_s = \sqrt{S}$ is the length of a square with the same surface as the measured uncarbonated area, which represents an average uncarbonated length, and Lsp is the length of the specimen (50 mm by default).

3.3 CO_2 content

The CO_2 content in the carbonated area was determined by thermogravimetric analysis (TGA). 20 g of samples were taken from the carbonated area revealed by the pH indicator and then crushed. TGA was performed with a Setaram Setsys Evolution 16/18 apparatus. Around 180 mg of the taken sample was heated from ambient temperature to 1000°C at a constant rate of 10°C/min under an argon atmosphere. The mass loss measured between 20°C and 100°C was attributed to the evaporation of free water, while, between 600°C and 975°C, it was attributed to the decarbonation of $CaCO_3$ [27,28]. The CO_2 content (C_{CO_2}) was expressed as a function of the sample mass after drying and decarbonation (equation 3). The increase in CO_2 content due to carbonation during the experiments, denoted ΔC_{CO_2}, was calculated by equation 4. The initial CO_2 content of the tested RA is due to the decarbonation of limestone particles and carbonated concrete particles present in the RA. The latter results from the natural carbonation which occurred during the service life of the concrete structures which were demolished, and during the storage of the RA after crushing on the recycling platform. The initial CO_2 content was found equal to 11%.

$$C_{CO_2} = \frac{\Delta m_{600-975°}}{m_{sample} - \Delta m_{20-100°C} - \Delta m_{600-975°}} \quad (3)$$

$$\Delta C_{CO_2} = C_{CO_2} - C_{CO_2}(t = 0) \quad (4)$$

Where $\Delta m_{20-100°C}$ is the loss of mass between 20 and 100°C; $\Delta m_{600-975°C}$ is the loss of mass due to decarbonation between 600 and 975°C; m_{sample} is the mass of a sample.

3.4 Effective CO_2 diffusion coefficient

The effective CO_2 diffusion coefficient of CRA was determined with the gas diffusion cell shown in Figure 5 [30]. Before testing, the specimen was embedded in a ring of resin and placed in the diffusion cell. During the test, two sensors continuously measured the CO_2 concentration in the upstream and downstream chambers, which were separated by the specimen. The CO_2 concentration in the upstream chamber was kept constant (5%) by regulation using a sensor and an electric valve. To avoid over-pressure, the upstream chamber remained open due to the presence of an outlet pipe. In the downstream chamber, the CO_2 concentration increased from zero (<0.05%) to 5%, because CO_2 was diffusing through the specimen.

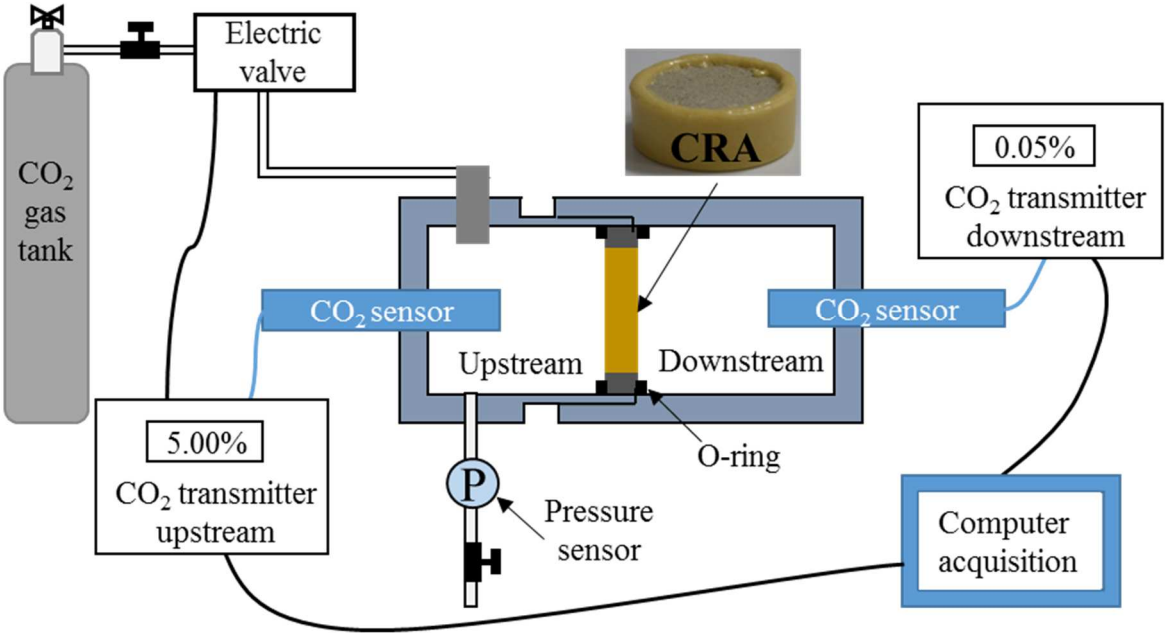

Figure 5: Set-up for CO_2 diffusion test.

To obtain the effective diffusion coefficient, we assume that the diffusion process is one dimensional at the macroscopic scale following the Fick's second law. Thus, the time-evolution of the CO_2 concentration in the downstream chamber can be calculated by the following equations system:

$$\begin{cases} \dfrac{\partial}{\partial t}(pC) = \dfrac{\partial}{\partial x}\left(D_{CO_2}\dfrac{\partial C}{\partial x}\right) \quad \forall x \in \Omega = [0, X_s], t \in [0, T] \\ C(x,0) = 0 \quad x \in \Omega \\ C(0,t) = C_{up} \quad t > 0 \\ \dfrac{\partial}{\partial t}C(X_s,t) = -D_{CO_2}\dfrac{\partial}{\partial x}C(X_s,t)\left(\dfrac{A_s}{V_{down}}\right) \quad t > 0 \end{cases} \tag{5}$$

With $C(x,t)$: the CO_2 concentration at location x and time t, p: the specimen porosity, D_{CO_2}: the effective CO_2 diffusion coefficient, X_s: the specimen thickness, T: the test duration, C_{up}: the CO_2 concentration in the upstream chamber, A_s: the specimen surface, and V_{down}: the volume of the downstream chamber.

The last equation expresses the boundary condition of the interface between the sample and the downstream chamber ($x=X_s$). Considering that the CO_2 diffusion in the air is much faster than in the specimen, it is assumed that the flow through the interface (A_s) is distributed immediately in the downstream chamber (V_{down}), where the CO_2 concentration remains homogeneous. The equations system is solved numerically using the finite elements method (FEniCs library https://fenicsproject.org/). The effective diffusion coefficient is obtained by minimising the difference between the experimental time-evolution of CO_2 concentration in the downstream and numerical examples.

An experimental campaign to determine the CO_2 diffusion coefficient was carried out on specimens CRA-H2 from the three natural carbonation enclosures. For each RH condition, three specimens were tested 30 days after compacting, when the mass of CRA was quasi-stable (moisture equilibrium). Each specimen was tested twice to verify eventual carbonation during the CO_2 diffusion test (as discussed in section 4.4).

4 Results and discussion

4.1 Microstructure

Figure 6 shows the desorption isotherms obtained on CRA and non-compacted RA by the GSA method and by the SSS method described in section 3.1. The “SSS” water contents were determined

at 90 days for 53%RH Nat, 65%RH Nat, and at 30 days for 95%RH Nat. At saturation, the water contents of the RA (w_{RA}) and the CRA (w_{CRA}) are 3.6% and 22%, respectively.

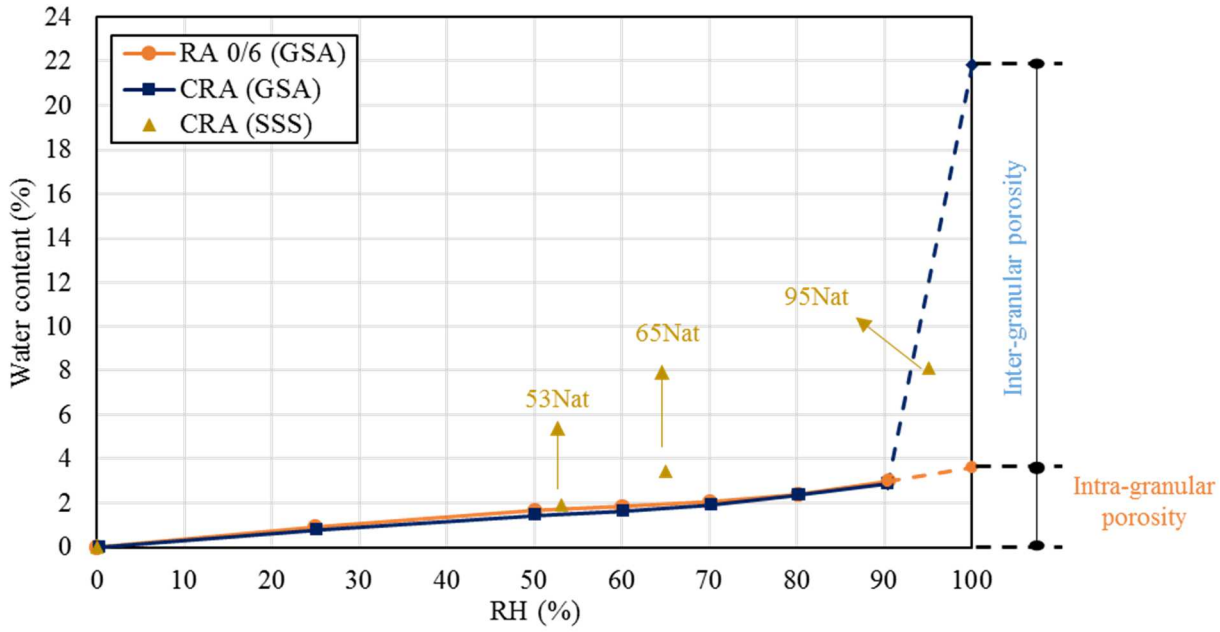

Figure 6: Desorption isotherms of CRA and RA 0/6 determined by two methods (GSA and SSS). The discontinuous lines were deduced from the water contents after immersion in water (100% RH) and the water contents at 90% RH.

The CRA desorption isotherm obtained by the GSA method is close to the isotherm obtained by the SSS method. We can also compare the isotherm of CRA and that of RA 0/6. For the latter, the water retention capacity is due to the porosity of the particles, while for CRA, water is stored in the porosity of the particles and in the inter-granular porosity. In the range of 0-90% RH, the two curves are similar. Therefore, if RH is less than 90%, the water in the CRA is mainly located in the intra-granular porosity.

The difference between the water content of the RA (w_{RA}) and that of the CRA (w_{CRA}) at 100% RH allows estimation of the total accessible water porosity (p) and the inter-granular porosity (p_{ig}):

$$w_{ig}=w_{CRA}-w_{RA} \quad (6)$$

$$p=\frac{w_{CRA}\times m_{dry}}{\rho_w \times V_{app}} \quad (7)$$

$$p_{ig} = \frac{w_{ig} \times m_{dry}}{\rho_w \times V_{app}} \quad (8)$$

where m_{dry} is the dry mass of a sample, and ρ_w the water density. The total porosity and inter-granular porosity values were found to be 38.1% and 31.9%, respectively. This latter value corresponds to the intended compactness of the CRA (i.e. 69%).

4.2 Mass variations of specimens

During manufacture, the CRA were compacted with 10% water content. According to the desorption isotherms (Figure 6), this water content corresponds to RH which is higher than or equal to 95% . This means that the CRA should dry in all three environments (53, 65, and 95% RH). Figure 7 shows the mass variations of CRA cured under the four conditions as a function of time.

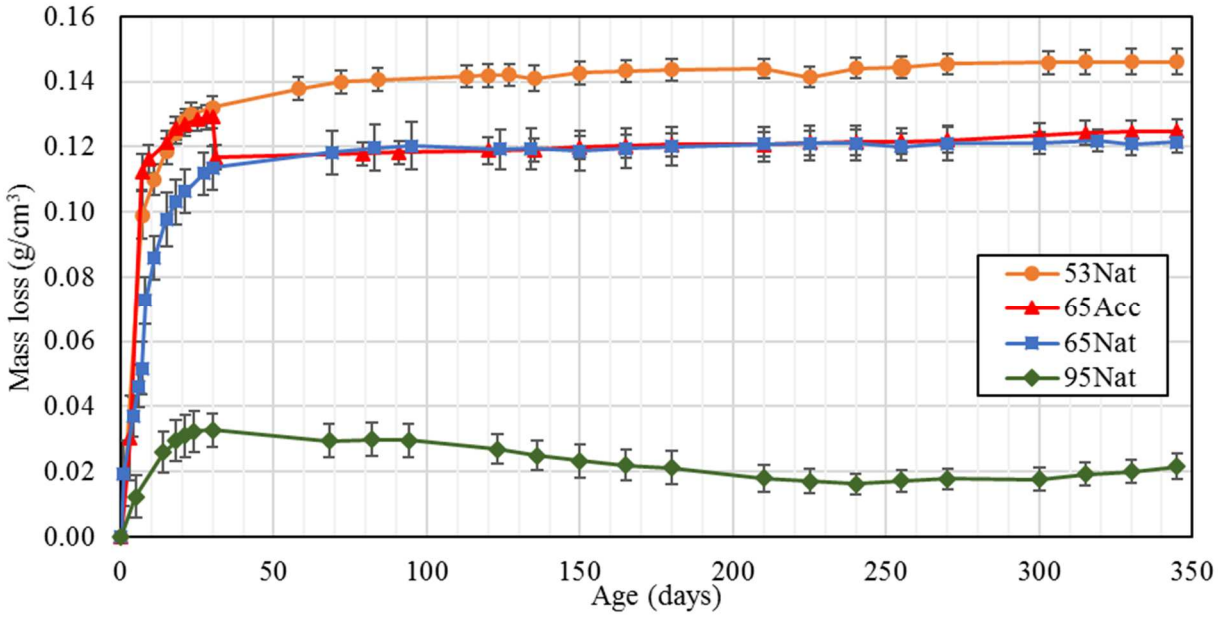

Figure 7: Mass loss per volume of specimens under different conditions.

The mass of all specimens is decreasing mostly in the first 30 days. Note that the specimens stored in the accelerated carbonation enclosure (65Acc) reach equilibrium faster than the specimens stored at the same RH but in natural conditions (65Nat). This faster drying kinetic is due to the ventilator in the accelerated carbonation enclosure. In the long term, the specimens conditioned under the 53Nat and 65 Nat & Acc continue to dry with a slower kinetic.

A particular point is observed for 65Acc when the CO_2 concentration is increased from 0.05% to 3% at 30 days. Specimen mass increases very quickly within one day, which is due to the accelerated carbonation of the cementitious matrix contained in the specimen. This point is discussed further in the next section of this paper.

A mass gain is observed after 30 days for the specimens placed in the 95% RH condition. Between 30 and 350 days, mass fluctuations of the specimens are observed in this environment. These variations could be due to the varied ambient condition since the RH in the enclosure is obtained by water. We also hypothesise that water exchanges between the inter and intra-granular porosities modify the total mass of the specimens.

To assess the distribution of water in a specimen, radial profiles of water content was determined on specimens 53Nat, as shown in Figure 8.

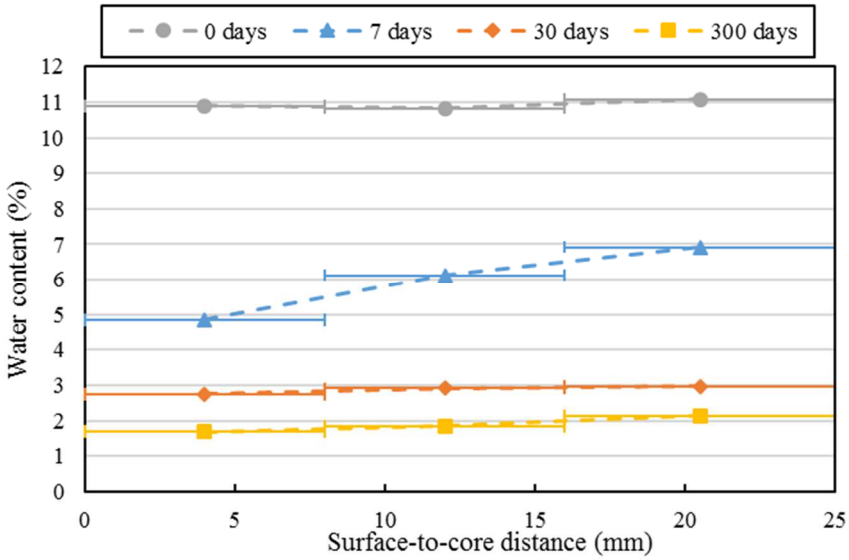

Figure 8: The average water content of 53Nat as a function of surface-to-inner portion distance.

In the beginning, the water content of the CRA is homogeneous and in line with expectations (11%). A gradient of water content is visible at 7 days. At 30 days, water content is constant across the radius. This confirms the strong mass loss between 0 and 30 days and shows that much of the inter-granular porosity has been dried out. Between 30 and 300 days, water content continues to decrease

almost uniformly throughout the specimen. This decrease corresponds to drying of the intra-granular porosity, because at 30 days the water content is about 3%, which is close to the saturation content of RA (w_{RA}). The analysis of the drying behaviour of RA and CRA illustrates the double porosity system of a compacted granular medium.

4.3 Carbonation depths

Figure 9 shows the time-evolution of the carbonation depths (Xc) of CRA determined with the pH indicator under natural and accelerated conditions. The four photographs show the carbonation depths on cross-sections after spraying of the phenolphthalein indicator at 180 days.

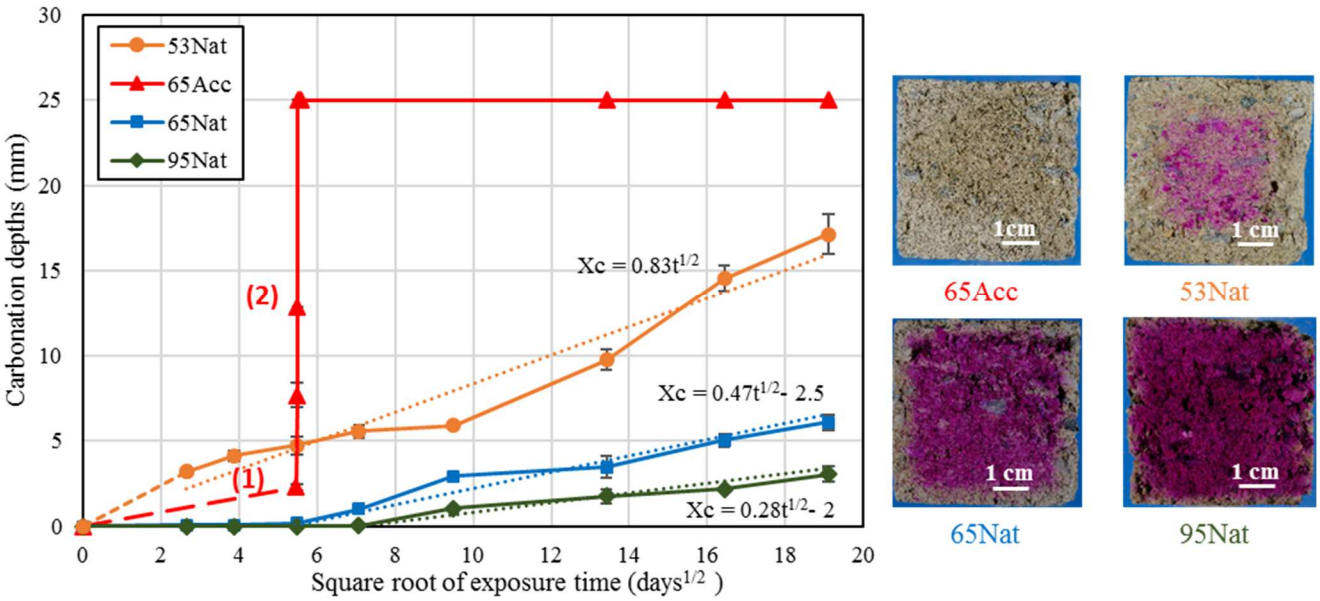

Figure 9: Carbonation depths (Xc) as a function of the square root of exposure time (left); Cross-section of the specimens after spraying the phenolphthalein alcoholic solution at 180 days (right).

Regardless of the RH in natural carbonation enclosures, CO_2 diffuses into the porous network, where it dissolves and acidifies the interstitial solution. In natural conditions, Xc is almost proportional to the square root of time, which is consistent with usual carbonation models based on Fick's first law [30], as shown in equations (9)-(10):

$$X_c(t) = A_c \cdot \sqrt{t} \qquad (9)$$

$$A_c = \sqrt{\frac{2D_{CO_2}[CO_2]}{Q_{CO_2}}} \quad (10)$$

with D_{CO_2} (m^2/s) the effective diffusion coefficient of CO_2, $[CO_2]$ (kg/m^3) the ambient CO_2 concentration, and Q_{CO_2} (kg/m^3) the content of carbonatable elements (per cubic meter of CRA).

This highlights that the observed phenomenon is controlled mainly by gas diffusion. The consumption of CO_2 by chemical reactions is much faster than CO_2 diffusion. Notably, carbonation depths measured with phenolphthalein are not a carbonation front (binding of CO_2), but a front that separates two zones with different pH values.

From our results, the carbonation rates A_c are estimated at 0.28 $mm/d^{1/2}$, 0.47 $mm/d^{1/2}$ and 0.83 $mm/d^{1/2}$ respectively, for 95Nat, 65Nat, and 53Nat. Note the presence of an offset from the origin for the 65% RH Nat and 95% RH Nat, which indicates that the carbonation does not begin immediately. Indeed, after compaction, the degree of saturation of the CRA samples is very high (see section 4.1). Since the CO_2 diffusion coefficient in the air is 10^4 times higher than the diffusion in water [31], there is minimal diffusion of CO_2 inside the specimen after compaction. Pores remain filled by water longer in the case of 65Nat and 95Nat, as confirmed by the drying curves shown in Figure 7.

For the 65Acc condition, two phases are observed (Figure 9). The first (1) is quite similar to what is observed in the natural carbonation enclosure (65Nat), since the experimental conditions (CO_2 concentration and RH) are almost identical in the first 30 days. Nevertheless, the ventilation in the accelerated carbonation enclosure results in higher drying and thus in a higher natural carbonation rate. The second phase (2) with a high CO_2 concentration (3%) is much faster. The CRA sample is completely carbonated within 8 hours according to the pH drop (see section 4.5).

4.4 CO_2 diffusion coefficient

Figure 10 compares the experimental and numerical time-evolutions of the relative CO_2 concentration (ratio of downstream to upstream concentrations). The first diffusion tests were carried

out just after the specimens were taken from the conservation enclosures (Figure 10a). The second diffusion tests were carried out on the same specimens just after the first diffusion tests (Figure 10b). The red curves are the numerical evolutions, which are calculated by minimisation to determine an effective diffusion coefficient.

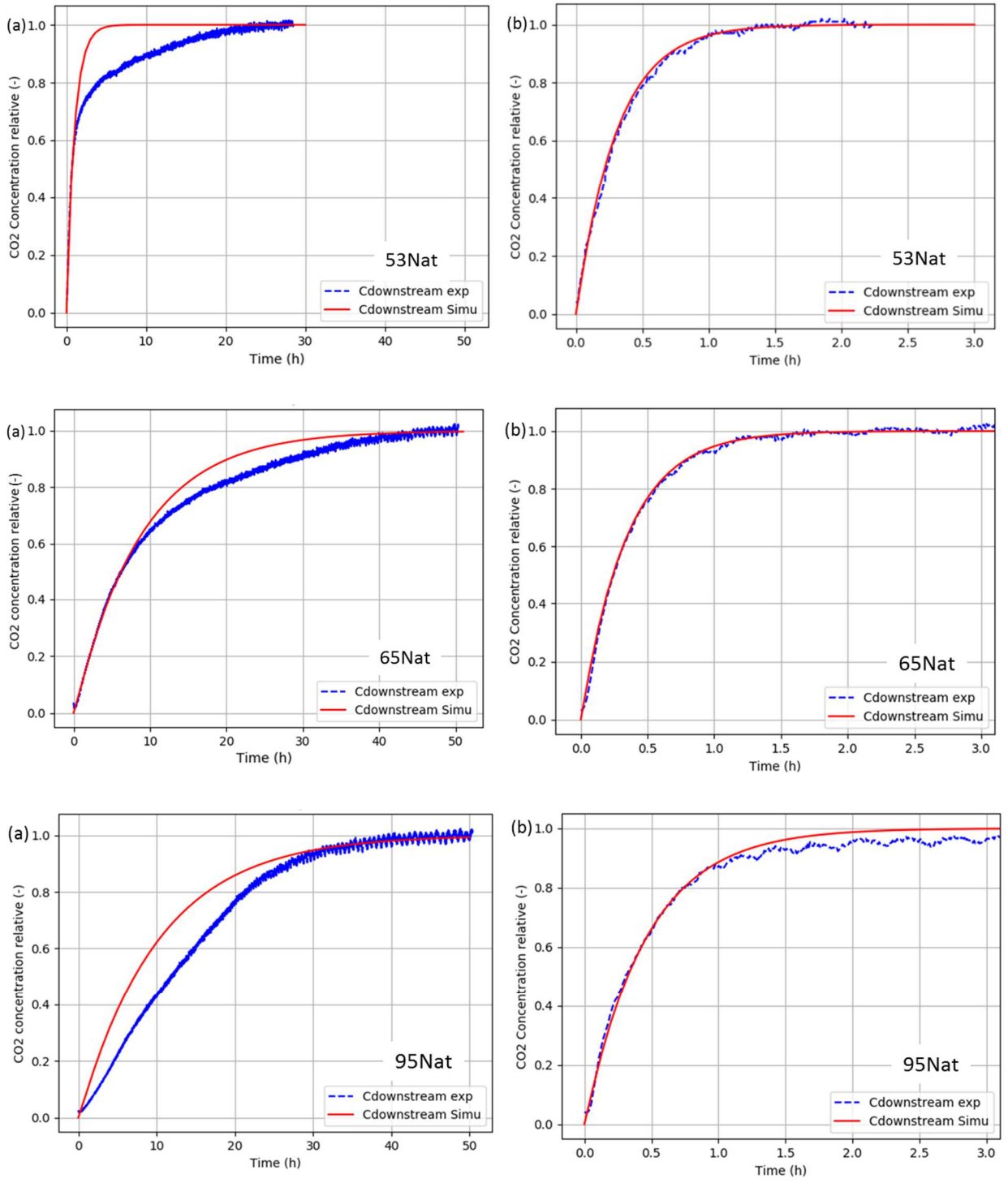

Figure 10: Comparison between numerical and experimental evolutions of CO_2 relative concentration for the first test (a) and second test (b).

We notice that the numerical curves for the first tests in Figure 10a do not match the experimental curves. This shows that, during the first diffusion tests, the observed phenomenon is not a Fickian diffusion. Indeed, the CO_2 is consumed by carbonisation during the diffusion through the CRA. To better approximate the experimental curve, a carbonation model should include at least one diffusion term and one CO_2 consumption term (reactive term). Although the phenomenon is a reactive transfer, an "apparent" diffusion coefficient was calculated and given in Table 4.

The second series of tests were carried out on the same samples that were tested previously. In this case, the time needed to reach the equilibrium CO_2 concentration between up and downstream (relative concentration equal to 1) is much shorter than during the first test (Figure 10b). Moreover, a good agreement is found between the numerical and experimental curves. This highlights that most of the carbonatable materials in the specimens were carbonated during the first test. The diffusion coefficients measured in this case are the coefficients of carbonated CRA or partially carbonated CRA, which are higher than the apparent coefficients deduced from the first tests, as expected (Table 4).

The diffusion coefficients are all of the same order of magnitude. The slight differences between 53Nat, 65Nat, and 95Nat are mainly due to differences in the degree of water saturation [32,33].

Table 4: CO_2 effective diffusion coefficients for 53Nat, 65Nat and 95Nat at 30 days.

CO_2 effective diffusion coefficient	**53Nat (10^{-8} m^2/s)**	**65Nat (10^{-8} m^2/s)**	**95Nat (10^{-8} m^2/s)**
First test	10.9 ± 1.2	2.9 ± 0.2	2.5± 0.2
Second test	62.7 ± 1.6	60.5 ± 0.8	45.0 ± 0.1

4.5 CO_2 content in the carbonated area

Figure 11a shows the evolution of the bound ΔC_{CO_2} content in the carbonated area for the CRA of the four enclosures, measured by TGA analysis. As a reminder, ΔC_{CO_2} content is the difference between the initial CO_2 content and CO_2 content determined at a given time.

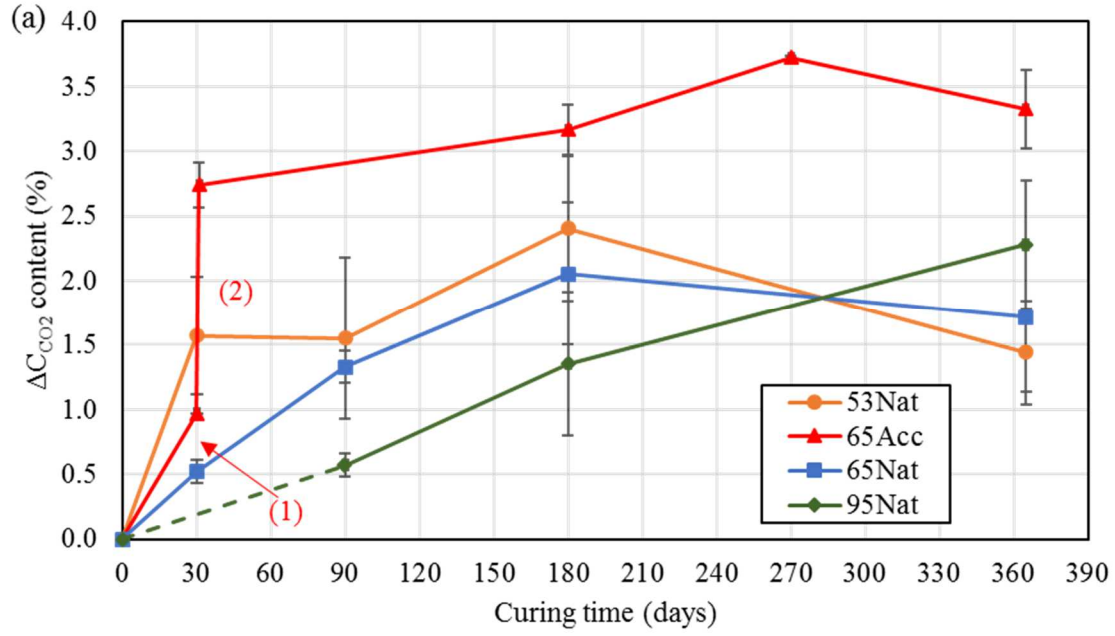

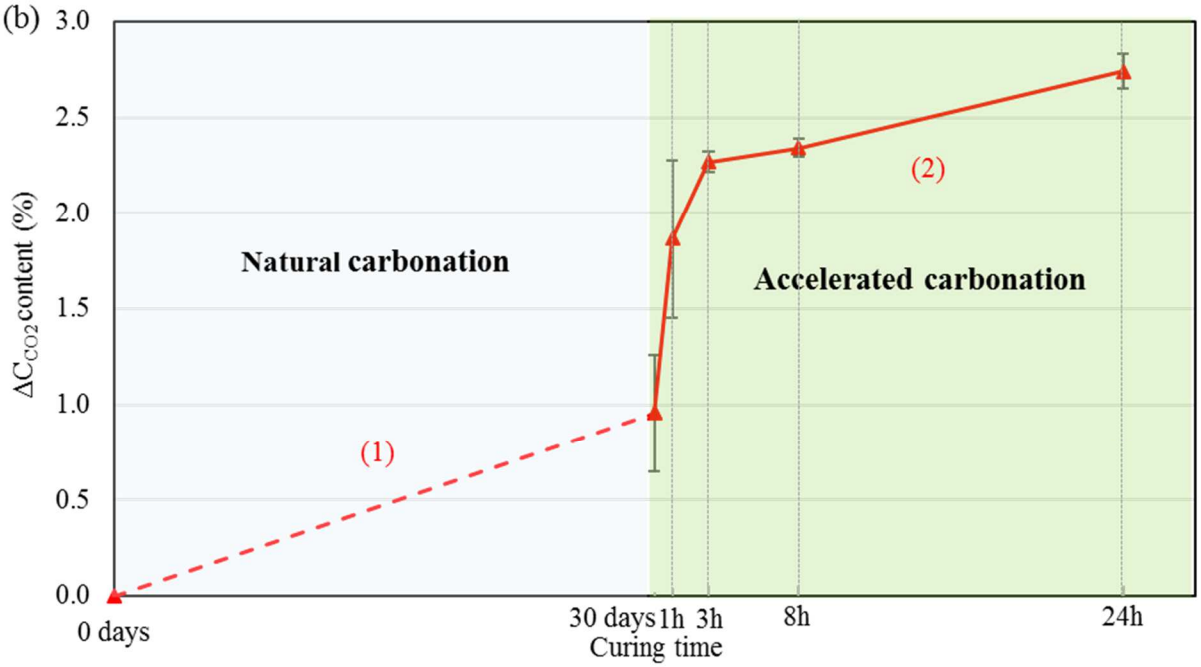

Figure 11: Variation of ΔC_{CO_2} content in the carbonated area under the different conditions (a); part (1) and (2) of 65Acc zoom (b).

TGA confirms the carbonation of the specimen under natural conditions whatever the RH, since the ΔC_{CO_2} content in the carbonated area increases. It should be borne in mind that the "carbonated area" is the area highlighted by the pH drop shown after phenolphthalein spraying. Thus, strictly speaking, it is not a fully carbonated area and the material in this area continues to uptake CO_2 even after the pH has dropped.

It is also noted that the CO_2 contents determined for natural conditions are a little scattered. This is due to sampling in the carbonated area, which is quite difficult to achieve because the carbonation depths are thin. In this area, the ΔC_{CO_2} content is probably not homogeneous. Figure 12 shows a profile of ΔC_{CO_2} for 65Nat. According to the pH indicator, the carbonation depth is about 8 mm. This profile confirms that in the carbonated area determined by the coloured indicator, the amount of CO_2 bound is not homogeneous. We also notice that the ΔC_{CO_2} content has increased beyond 8 mm: the CO_2 has already reached the core of the CRA by diffusion.

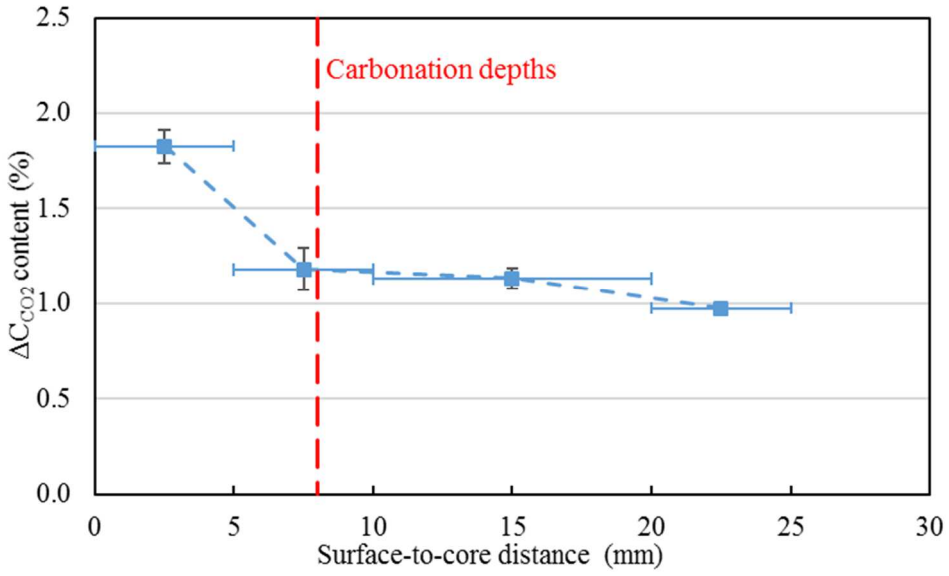

Figure 12: Radial profile of ΔC_{CO_2} content bound for 65Nat

In the long term, the CO_2 content is rather stable for 53% and 65% RH, while for 95% RH, the content is still increasing. This slow but continuous increase may be due to the higher quantity of potentially carbonatable materials at 95% RH, because the water content is higher than the other two ambiances [34].

Figure 11a also gives the evolution of ΔC_{CO_2}content for the 65Acc. The increase ΔC_{CO_2} is very fast when CO_2 is injected into the carbonation chamber at 30 days. It is also noted that more CO_2 is bound under the accelerated conditions than under natural carbonation (phase (1)), showing the influence of CO_2 concentration on the binding capacity of cementitious material.

Figure 11b focuses on the evolution of ΔC_{CO_2}content for the 65Acc when the CO_2 concentration was increased (phases (1) and (2)). In the 65Acc enclosure, the variation of CO_2 content in the carbonated area can be divided into two phases: (1) natural carbonation over 30 days, (2) accelerated carbonation within 24 hours. In the second phase, in the first 3 hours, the CO_2 content increases sharply, from 1% to 2.3%, and then the carbonation rate slows down; the CO_2 content increases from 2.3% to 2.7% between 3h to 24h. The carbonation rate decreases with the carbonation degree of the material, as observed in the case of carbonation of pure cementitious phases [19]. This slowdown is usually explained by the carbonate layer produced on the surface of reactive phases. This progressive covering hinders the diffusion of ions (especially Ca^{2+}) which prevents further carbonation [35,36]. However, after 24 hours, the carbonation rate remains positive. Inside the area revealed by pH drop, CO_2 uptake continues slowly over time.

As is known, the binding of CO_2 modifies the mass of the specimen. Therefore, we can evaluate a correlation between the evolution of CO_2 content and the evolution of mass. During the 24 hours of accelerated carbonation, the mass of the specimen increases by 1.5g (knowing that the mass gain is 0.015g/cm^3, as shown in Figure 7):

$$m_{gain\,m} = V_t \times \varepsilon = 1.5\text{g} \qquad (11)$$

This measured mass gain ($m_{gain\,m}$) can be compared to the theoretical mass gain ($m_{gain\,t}$) due to CO_2 fixation. The latter is calculated as follows:

$$m_{CRA\,dry,decarbonated} = m_{dry} \times (1 - C_{CO_2}(t = 0)) = 149.2\text{g} \quad (12)$$

$$m_{gain\,t} = \Delta C_{CO_2} \times m_{CRA\,dry,decarbonated} = 2.6\text{g} \quad (13)$$

Where: $m_{CRA\,dry,decarbonated}$ is the initial mass of dried and decarbonated CRA, calculated with the dry mass (m_{dry}) and the CO_2 content before accelerated carbonation $C_{CO_2}(t = 0)$. ΔC_{CO_2} is the increased CO_2 content due to accelerated carbonation, which equals 1.7%, as shown in Figure 11b. These simple evaluations show that the measured mass gain is less than the theoretical mass gain because of CO_2 absorption. This difference may be due to the drying of CRA during accelerated carbonation. The carbonation of cement hydrates, especially portlandite, causes a water release that will be removed by drying [37].

To further illustrate, we have determined the desorption isotherm of CRA after one year of accelerated carbonation. The desorption isotherm was determined by placing carbonated CRA in 3 enclosures (53Nat, 65Nat, and 95 Nat). Figure 13 shows the isotherm of CRA before carbonation and after carbonation by the SSS method.

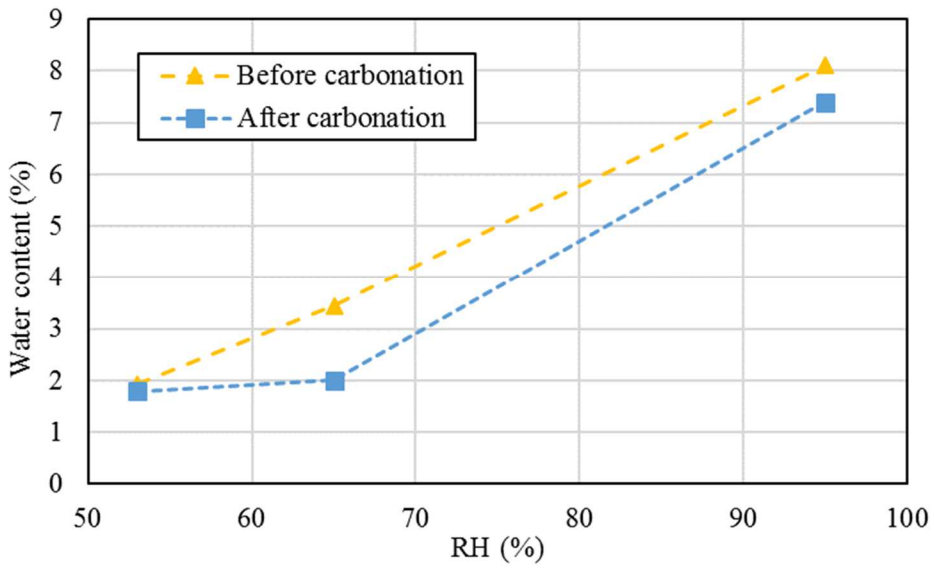

Figure 13: Desorption isotherm of CRA before carbonation and after carbonation by SSS method.

We note that the water retention capacity decreases after carbonation, especially at 65% RH (Figure 13). This is consistent with the results in the literature, which show isothermal changes, especially in the capillary pore range, which are explained by the decrease in porosity of the cementitious material [32,38–40]. In the case of CRA, carbonation mainly reduces the intra-granular porosity, because for 65% RH the content at a water equilibrium is changed.

The comparison between theoretical and measured mass gain finally shows that the determination of mass variation during carbonation is not sufficient to quantify the CO_2 uptake by recycled aggregates.

4.6 Discussion

Nowadays, RA are mainly used for unbound sub-base layers of pavement. The present study confirms that the carbonation effect of RA is not negligible, even if they are mainly composed of old crushed concrete particles. It reveals however that their carbonation rate when compacted is relatively low. Indeed, the carbonation rate was found to be between 0.28 mm/day$^{1/2}$ and 0.83 mm/day$^{1/2}$, i.e. 5 mm/year$^{1/2}$ and 16 mm/year$^{1/2}$, for high and low water contents respectively. It is interesting to note that these carbonation rates are of the same order of magnitude as those for a low strength concrete proposed to predict carbonation depth in the European Standard NF EN 16757 [41] (namely 6 mm/year$^{1/2}$ and 17 mm/year$^{1/2}$ for surfaces exposed to rain and those in a dry climate, respectively).

The first parameter to explain the relatively low carbonation rate of CRA is the CO_2 diffusion coefficient, which is a key parameter in equation 14. Many models have been proposed to predict the gas diffusion coefficient of a porous material, knowing the porosity, the water saturation degree, and the type of gas, e.g. Kristensen et al.[42]. To our knowledge, the most popular model is Millington's [43], which writes as follows:

$$\frac{D}{D_0} = p^a(1-S)^b \qquad (14)$$

with: D_0 the diffusion coefficient of the gas in the air, p the porosity, S the water saturation degree, and a and b constant.

Millington and Quirk [44] proposed values for the exponents a and b to predict the diffusivity of granular soils. Values were also proposed by Thiery et al. [45] for cementitious materials such as mortar and concrete. From these values, relative diffusivities D/D_0 of two types of materials, soils, and cement-based materials, were calculated using the porosity and the water saturation degrees of the CRA tested in the present study (Table 5). In Figure 14, we compare the obtained relative diffusivities determined for the tested CRA (D_0, i.e. the diffusion coefficient of CO_2 in air was taken to $1.6.10^{-5}$ m²/s). It clearly appears that the diffusion coefficient of the porous media formed by compacted recycled aggregates is in the same order of magnitude as the diffusion coefficient of cement-based materials. This explains why the carbonation rate of CRA is close to the rate of low-strength concrete.

Table 5: Assessment of the relative gas diffusivity D/D_0 for granular soils and cementitious materials based on Millington's model (equation (14)). Degrees of water saturation S were determined just before diffusion tests, i.e. at 30 days of drying.

Material type	**Reference**	**a**	**b**	p	**53Nat**		**65Nat**		**95Nat**	
					S	**D/D_0**	**S**	**D/D_0**	**S**	**D/D_0**
Granular soils	Millington and Quirk [44]	1.33	3.33	0.38	0.16	0.156	0.19	0.139	0.44	0.039
Cementitious materials	Thiery et al, 2007 [45]	2.74	4.20	0.38	0.16	0.034	0.19	0.030	0.44	0.006

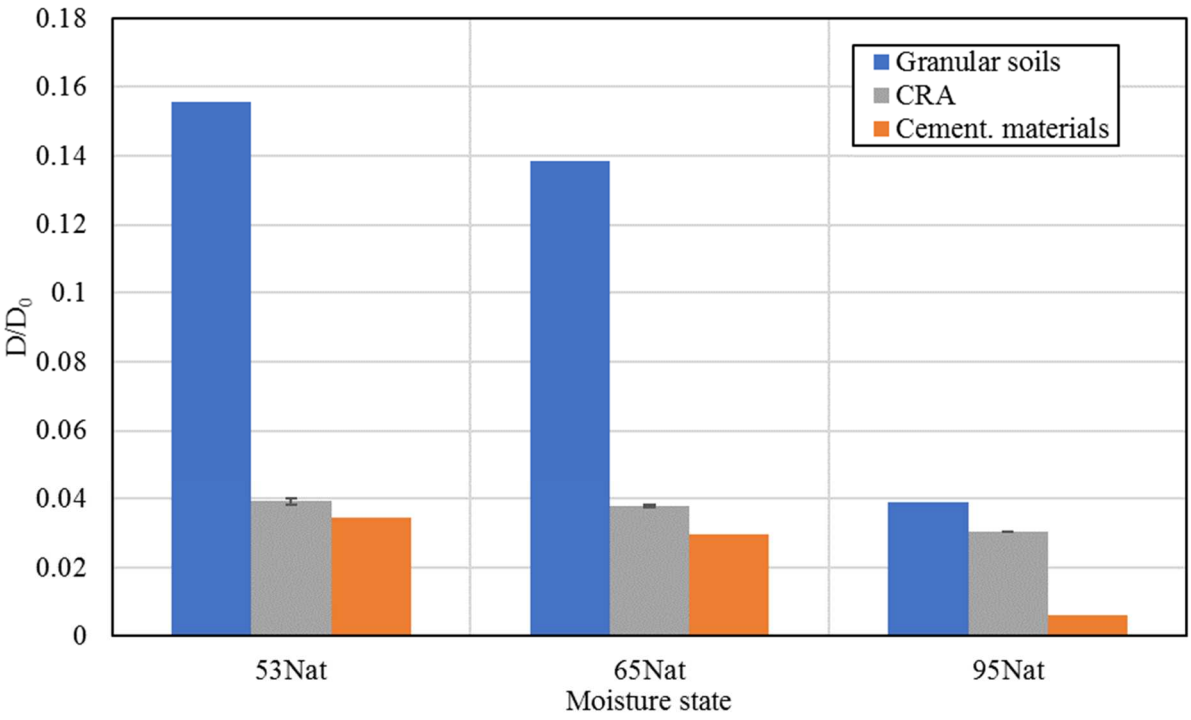

Figure 14: Relative diffusivities of the tested CRA compared to relative diffusivities assessed for two types of porous materials using Millington model (Table 5).

Another parameter to be analysed regarding the carbonation rate is the amount of carbonatable compounds in the material. After one year of carbonation, the increase of CO_2 content in the area given by the pH indicator was between 2% (natural conditions) and 3.5% (accelerated conditions), as shown in Figure 11. This corresponds to a CO_2 binding capacity between 30 kg (natural conditions) and 53 kg (accelerated conditions) per m^3 of CRA (depending on the pH). In a concrete mixture, the cement content is usually around 300 kg/m^3. Portland cement (type CEM I or CEM II), which is the most commonly used cement, has a mass content of calcium oxide of about 60%. Therefore, the CO_2 binding capacity of concrete can be estimated at around 140 kg/m^3. Since it is unlikely that all the calcium oxides can be fully carbonated, as discussed previously in section 4.5, this value should be seen as a maximal capacity. In reality, the CO_2 binding capacity of Portland cement concrete could be 2 times lower [19], i.e., 70 kg/m^3. In the case of the tested CRA, the CO_2 binding in a natural condition (30 kg/m^3) is only 2 times lower than this order of magnitude. This means that CRA have a non-negligible CO_2 binding capacity in atmospheric conditions, compared to concrete. In addition to

the low diffusion coefficient, this explains why the progression of the carbonation front inside CRA is slow, with a carbonation rate close to rates usually observed for concrete with low cement content.

The carbonation rate of compacted recycled aggregates is in the order of a few millimetres per year. Knowing this order of magnitude brings us to several applications. First, in the context of road construction, carbonation cannot be the physico-chemical phenomenon resulting in the rapid evolution of the mechanical properties of CRA layers often observed in situ during the first months after compaction [46]. Indeed, the core of a CRA layer several centimetres thick cannot be impacted by carbonation over this short period.

Second, from an environmental point of view, the CO_2 uptake by a layer made of compacted recycled aggregates is slow. From the carbonation rates and the CO_2 binding capacity determined in the present study, the CO_2 utpake is between 0.15 and 0.48 kg per m^2 of RA layer per $year^{1/2}$. Thus, if RA are to be used as a carbon sink, it is preferable to carbonate them before compacting. Processes with conditions accelerating carbonation, i.e. high concentration of CO_2 and moving bed reactors, are undoubtedly more relevant, e.g., [47].

Finally, the main concern of RA used in road layers may be the impact of their high pH leachate on groundwater or metal pipes. As claimed by Gupta et al.[48], the carbonation of RA could be a way to mitigate these impacts. However, carbonation in situ would be too slow for such a beneficial effect. Again, it would be better to carbonate RA before their use in road construction, if carbonation is considered as a way to reduce the pH of leachate.

5 Conclusions

This study investigated the carbonation of recycled aggregates compacted for road construction. Experimentations on compacted samples of a recycled sand from an industrial crushing platform allowed us obtaining the following results:

- The CO_2 binding capacity due to natural carbonation was found to be significant, i.e. about 30kg per m^3 of compacted recycled aggregates . Small differences were found between the

binding capacities determined in the three tested ambient relative humidities (53, 65, and 95% RH).

- In atmospheric conditions, the carbonation front revealed by a pH indicator was found to be proportional to the square root of time, as classically observed for concrete. The carbonation rate was also found to depend on the ambient relative humidity. The rates were of the same order of magnitude as those of low strength concretes, i.e. a few tens of mm/year$^{1/2}$.
- The low carbonation rate of the tested compacted recycled sand samples can be explained by both their small diffusion coefficient and their high CO_2 binding capacity.
- In accelerated conditions, i.e. carbonation at 3% CO_2 concentration, both carbonation rate and CO_2 binding capacity increase significantly.

From these results, it can be concluded that the carbonation of a road layer made of compacted recycled aggregates will be quite slow. Therefore, all possible benefits from carbonation, such as CO_2 uptake or reduction of pH leachates, will not be achieved quickly over the service life of the road. For such benefits, it would be better to carbonate the recycled aggregates prior to placing, for instance with industrial gases of high CO_2 concentration, as proposed in the French national project FastCarb.

In addition to investigations on the accelerated carbonation of recycled aggregates, other studies should also focus on atmospheric carbonation during the storage period in crushing platforms.

Acknowledgment

This work was supported by the French Environment and Energy Management Agency (ADEME) and the Region Nouvelle-Aquitaine (France).

References

[1] J.D. Lau Hiu Hoong, J. Lux, P.-Y. Mahieux, P. Turcry, A. Aït-Mokhtar, Determination of the composition of recycled aggregates using a deep learning-based image analysis, Autom. Constr. 116 (2020) 103204. https://doi.org/10.1016/j.autcon.2020.103204.

[2] D. François, A. Jullien, J.P. Kerzreho, L. Chateau, Full-scale experimentations on alternative materials in roads: analysis of study practices, Waste Manag. 29 (2009) 1076–1083. https://doi.org/10.1016/j.wasman.2008.08.007.

[3] D. François, A. Jullien, A framework of analysis for field experiments with alternative materials in road construction, Waste Manag. 29 (2009) 374–382. https://doi.org/10.1016/j.wasman.2008.04.005.

[4] C.S. Poon, D. Chan, Feasible use of recycled concrete aggregates and crushed clay brick as unbound road sub-base, Constr. Build. Mater. 20 (2006) 578–585. https://doi.org/10.1016/j.conbuildmat.2005.01.045.

[5] L. Garach, M. López, F. Agrela, J. Ordóñez, J. Alegre, J. Moya, Improvement of Bearing Capacity in Recycled Aggregates Suitable for Use as Unbound Road Sub-Base, Materials. 8 (2015) 8804–8816. https://doi.org/10.3390/ma8125493.

[6] I. Vegas, J.A. Ibañez, A. Lisbona, A. Sáez de Cortazar, M. Frías, Pre-normative research on the use of mixed recycled aggregates in unbound road sections, Constr. Build. Mater. 25 (2011) 2674–2682. https://doi.org/10.1016/j.conbuildmat.2010.12.018.

[7] L. Chai, C.L. Monismith, J. Harvey, Re-cementation of Crushed Material in Pavement Bases, University of California Pavement Research Center, 2009. https://escholarship.org/content/qt7wt5j1n3/qt7wt5j1n3_noSplash_69794770abcca92b05ba2c036c4c70e3.pdf.

[8] C.-S. Poon, X.C. Qiao, D. Chan, The cause and influence of self-cementing properties of fine recycled concrete aggregates on the properties of unbound sub-base, Waste Manag. 26 (2006) 1166–1172. https://doi.org/10.1016/j.wasman.2005.12.013.

[9] M. Fernández Bertos, S.J.R. Simons, C.D. Hills, P.J. Carey, A review of accelerated carbonation technology in the treatment of cement-based materials and sequestration of CO2, J. Hazard. Mater. 112 (2004) 193–205. https://doi.org/10.1016/j.jhazmat.2004.04.019.

[10] S. Kashef-Haghighi, Y. Shao, S. Ghoshal, Mathematical modeling of CO2 uptake by concrete during accelerated carbonation curing, Cem. Concr. Res. 67 (2015) 1–10. https://doi.org/10.1016/j.cemconres.2014.07.020.

[11] T. Kikuchi, Y. Kuroda, Carbon dioxide uptake in demolished and crushed concrete, J. Adv. Concr. Technol. 9 (2011) 115–124. https://doi.org/10.3151/jact.9.115.

[12] H. El-Hassan, Y. Shao, Carbon Storage through Concrete Block Carbonation, J. Clean Energy Technol. (2014) 287–291. https://doi.org/10.7763/JOCET.2014.V2.141.

[13] S.K. Kaliyavaradhan, T.-C. Ling, Potential of CO2 sequestration through construction and demolition (C&D) waste—An overview, J. CO2 Util. 20 (2017) 234–242. https://doi.org/10.1016/j.jcou.2017.05.014.

[14] D. Xuan, B. Zhan, C.S. Poon, Assessment of mechanical properties of concrete incorporating carbonated recycled concrete aggregates, Cem. Concr. Compos. 65 (2016) 67–74. https://doi.org/10.1016/j.cemconcomp.2015.10.018.

[15] B. Zhan, C. Poon, C. Shi, CO2 curing for improving the properties of concrete blocks containing recycled aggregates, Cem. Concr. Compos. 42 (2013) 1–8. https://doi.org/10.1016/j.cemconcomp.2013.04.013.

[16] J. Zhang, C. Shi, Y. Li, X. Pan, C.-S. Poon, Z. Xie, Performance Enhancement of Recycled Concrete Aggregates through Carbonation, J. Mater. Civ. Eng. 27 (2015) 04015029. https://doi.org/10.1061/(ASCE)MT.1943-5533.0001296.

[17] B. Zhan, C.S. Poon, Q. Liu, S. Kou, C. Shi, Experimental study on CO2 curing for enhancement of recycled aggregate properties, Constr. Build. Mater. 67 (2014) 3–7. https://doi.org/10.1016/j.conbuildmat.2013.09.008.

[18] D. Xuan, B. Zhan, C.S. Poon, Development of a new generation of eco-friendly concrete blocks by accelerated mineral carbonation, J. Clean. Prod. 133 (2016) 1235–1241. https://doi.org/10.1016/j.jclepro.2016.06.062.

[19] M. Boumaaza, B. Huet, P. Turcry, A. Aït-Mokhtar, The CO2-binding capacity of synthetic anhydrous and hydrates: Validation of a test method based on the instantaneous reaction rate, Cem. Concr. Res. 135 (2020) 106113. https://doi.org/10.1016/j.cemconres.2020.106113.

[20] M. Sereng, A. Djerbi, O.O. Metalssi, P. Dangla, J.-M. Torrenti, Improvement of Recycled Aggregates Properties by Means of CO2 Uptake, Appl. Sci. 11 (2021) 6571. https://doi.org/10.3390/app11146571.

[21] X. Fang, D. Xuan, C.S. Poon, Empirical modelling of CO2 uptake by recycled concrete aggregates under accelerated carbonation conditions, Mater. Struct. 50 (2017). https://doi.org/10.1617/s11527-017-1066-y.

[22] E. Drouet, S. Poyet, P. Le Bescop, J.-M. Torrenti, X. Bourbon, Carbonation of hardened cement pastes: Influence of temperature, Cem. Concr. Res. 115 (2019) 445–459. https://doi.org/10.1016/j.cemconres.2018.09.019.

[23] N. Lippiatt, T.-C. Ling, S.-Y. Pan, Towards carbon-neutral construction materials: Carbonation of cement-based materials and the future perspective, J. Build. Eng. 28 (2020) 101062. https://doi.org/10.1016/j.jobe.2019.101062.

[24] NF EN 933-11, Tests for geometrical properties of aggregates - Part 11: classification test for the constituents of coarse recycled aggregate, (2009).

[25] NF EN 13286-53, Unbound and hydraulically bound mixtures - Part 53: methods for the manufacture of test specimens of hydraulically bound mixtures using axial compression, (2005).

[26] NF P 94-102-1, Soils: investigation and testing - Soil treated with hydraulic binder, possibly combined with lime, for use as a selected fill - Part 1: definition - Composition – Classification, (2001).

[27] V.S. Ramachandran, M.P. Ralph, J.J. Bausoin, A.H. Delgado, eds., Handbook of thermal analysis of construction materials, Noyes Publ., Andrew, Norwich, NY, 2002.

[28] G. Villain, M. Thiery, G. Platret, Measurement methods of carbonation profiles in concrete: Thermogravimetry, chemical analysis and gammadensimetry, Cem. Concr. Res. 37 (2007) 1182–1192. https://doi.org/10.1016/j.cemconres.2007.04.015.

[29] F. Gendron, P. Turcry, A. Aît-Mokhtar, Coefficient de diffusion du CO2 de pâtes de ciment - étude expérimentale de l'influence de la nature du liant et d'une carbonatation accélérée, in: AFM, Association Française de Mécanique, Lille, France 28 Août au 1er Septembre 2017, 2017. http://hdl.handle.net/2042/63471.

[30] V.G. Papadakis, C.G. Vayenas, M.N. Fardis, A reaction engineering approach to the problem of concrete carbonation, AIChE J. 35 (1989) 1639–1650. https://doi.org/10.1002/aic.690351008.

[31] D.R. Lide, G. Baysinger, S. Chemistry, L.I. Berger, R.N. Goldberg, H.V. Kehiaian, CRC Handbook of Chemistry and Physics, (2005) 2661.

[32] Y.F. Houst, F.H. Wittmann, Influence of porosity and water content on the diffusivity of CO2 and O2 through hydrated cement paste, Cem. Concr. Res. 24 (1994) 1165–1176. https://doi.org/10.1016/0008-8846(94)90040-X.

[33] C. Boher, F. Frizon, S. Lorente, F. Bart, Influence of the pore network on hydrogen diffusion through blended cement pastes, Cem. Concr. Compos. 37 (2013) 30–36. https://doi.org/10.1016/j.cemconcomp.2012.12.009.

[34] M. Boumaaza, P. Turcry, B. Huet, A. Aït-Mokhtar, Influence of carbonation on the microstructure and the gas diffusivity of hardened cement pastes, Constr. Build. Mater. 253 (2020) 119227. https://doi.org/10.1016/j.conbuildmat.2020.119227.

[35] I. Galan, F.P. Glasser, D. Baza, C. Andrade, Assessment of the protective effect of carbonation on portlandite crystals, Cem. Concr. Res. 74 (2015) 68–77. https://doi.org/10.1016/j.cemconres.2015.04.001.

[36] H.Y. Sohn, J. Szekely, The effect of intragrain diffusion on the reaction between a porous solid and a gas, Chem. Eng. Sci. 29 (1974) 630–634. https://doi.org/10.1016/0009-2509(74)80076-X.

[37] A. Morandeau, M. Thiéry, P. Dangla, Investigation of the carbonation mechanism of CH and C-S-H in terms of kinetics, microstructure changes and moisture properties, Cem. Concr. Res. 56 (2014) 153–170. https://doi.org/10.1016/j.cemconres.2013.11.015.

[38] M. Auroy, S. Poyet, P. Le Bescop, J.-M. Torrenti, T. Charpentier, M. Moskura, X. Bourbon, Comparison between natural and accelerated carbonation (3% CO2): Impact on mineralogy, microstructure, water retention and cracking, Cem. Concr. Res. 109 (2018) 64–80. https://doi.org/10.1016/j.cemconres.2018.04.012.

[39] V.T. Ngala, C.L. Page, Effects of carbonation on pore structure and diffusional properties of hydrated cement pastes, Cem. Concr. Res. 27 (1997) 995–1007. https://doi.org/10.1016/S0008-8846(97)00102-6.

[40] G. Villain, M. Thiery, Impact of carbonation on microstructure and transport properties of concrete, in: Lyon, France April 17-20 2005, 2005. https://www.irbnet.de/daten/iconda/CIB_DC24720.pdf.

[41] NF EN 16757, Sustainability of construction works - Environmental product declarations - Product category rules for concrete and concrete elements, (2017).

[42] A.H. Kristensen, A. Thorbjørn, M.P. Jensen, M. Pedersen, P. Moldrup, Gas-phase diffusivity and tortuosity of structured soils, J. Contam. Hydrol. 115 (2010) 26–33. https://doi.org/10.1016/j.jconhyd.2010.03.003.

[43] R.J. Millington, Gas Diffusion in Porous Media, Science. 130 (1959) 100–102. https://doi.org/10.1126/science.130.3367.100-a.

[44] R.J. Millington, J.P. Quirk, Permeability of porous solids, Trans. Faraday Soc. 57 (1961) 1200. https://doi.org/10.1039/tf9615701200.

[45] M. Thiery, G. Villain, P. Dangla, G. Platret, Investigation of the carbonation front shape on cementitious materials: Effects of the chemical kinetics, Cem. Concr. Res. 37 (2007) 1047–1058. https://doi.org/10.1016/j.cemconres.2007.04.002.

[46] J.D. Lau Hiu Hoong, Y. Hou, P. Turcry, P.-Y. Mahieux, H. Hamdoun, O. Amiri, J. Lux, A. Aït-Mokhtar, Reactivity of Recycled Aggregates Used for Pavement Base: From Field to Laboratory, J. Mater. Civ. Eng. 33 (2021) 04021129. https://doi.org/10.1061/(ASCE)MT.1943-5533.0003661.

[47] G.S. Dos Reis, B.G. Cazacliu, R. Artoni, J. Torrenti, Effect of the accelerated carbonation treatment on the recycled sand physicochemical characteristics through the rolling carbonation process, J. CO2 Util. 39 (2020) 101181. https://doi.org/10.1016/j.jcou.2020.101181.

[48] N. Gupta, M. Kluge, P.A. Chadik, T.G. Townsend, Recycled concrete aggregate as road base: Leaching constituents and neutralization by soil Interactions and dilution, Waste Manag. 72 (2018) 354–361. https://doi.org/10.1016/j.wasman.2017.11.018.